



Formation of hexagonal $\text{NaAl}_3\text{Si}_3\text{O}_{11}$ (NAS) phase, the Na end-member of hexagonal $\text{CaAl}_4\text{Si}_2\text{O}_{11}$ (CAS) phase, near 23 GPa above 2373 K in the compositions of $\text{NaAl}_3\text{Si}_3\text{O}_{11}$ and $\text{NaAlSi}_3\text{O}_8$

Youmo Zhou¹ · Tetsuo Irifune^{1,2}

Received: 24 March 2020 / Accepted: 28 July 2020 / Published online: 9 August 2020
© Springer-Verlag GmbH Germany, part of Springer Nature 2020

Abstract

Phase relations of $\text{NaAl}_3\text{Si}_3\text{O}_{11}$ and $\text{NaAlSi}_3\text{O}_8$ were explored at pressures of 20.5–23.5 GPa and temperatures of 2373 and 2573 K by multianvil experiments. For $\text{NaAl}_3\text{Si}_3\text{O}_{11}$, a new phase, which is tentatively named NAS phase, was obtained at 22.5 GPa, 2373 and 2573 K and also at 23.5 GPa, 2573 K. NAS phase was found to be isostructural to $\text{CaAl}_4\text{Si}_2\text{O}_{11}$ (CAS) phase, but have smaller lattice parameters. The other phase assemblages obtained for $\text{NaAl}_3\text{Si}_3\text{O}_{11}$ at 2373 K are jadeite + corundum + stishovite and NaAlSiO_4 calcium ferrite-type (CF) phase + corundum + stishovite. Our results suggest that NAS phase is stable around 23 GPa above 2373 K, while its stability region is much narrower than that of CAS phase in both pressure and temperature. Based on our results, the CAS–NAS solid solution with a Na/Ca ratio close to that of the Na-rich CAS phase (74:26) found in the shocked Martian meteorites can be stabilized around 23 GPa at temperatures below 2373–2573 K. For $\text{NaAlSi}_3\text{O}_8$, the phase assemblages of jadeite + stishovite and CF phase + stishovite were obtained at 20.5–23.5 GPa and 2373 K, while partial melting occurred at 2573 K, accompanied by the liquidus phase assemblages of stishovite + NAS phase and stishovite + corundum at 22.5 and 23.5 GPa, respectively. Stishovite and NAS phase are the residual solid phases in the partial melting of $\text{NaAlSi}_3\text{O}_8$. This result is supportive to the previous inference that the phase assemblage of stishovite + Na-rich CAS phase observed in the melt pockets of the shocked Martian meteorites was formed by a rapid crystallization of a high-pressure labradorite melt.

Keywords Aluminosilicate · Hexagonal $\text{CaAl}_4\text{Si}_2\text{O}_{11}$ phase · Hexagonal $\text{NaAl}_3\text{Si}_3\text{O}_{11}$ phase · Phase relation · Multianvil experiment

Introduction

Experimental studies showed that $\text{CaAl}_4\text{Si}_2\text{O}_{11}$ (CAS) phase with a hexagonal barium ferrite-type structure (Gautron et al. 1999) occurred in some continental crust materials at the mantle transition region pressures and temperatures of 1673–2173 K (Irifune et al. 1994; Ishii et al. 2012; Nishi

et al. 2018) and also in the partial melting of some basaltic materials at 25–27 GPa (Wang and Takahashi 1999; Hirose and Fei 2002; Kuwahara et al. 2018). The CAS phase observed in these previous studies was found to deviate chemically from pure CAS composition and contain less than 2 wt % Na_2O components. In contrast, CAS phase with a Na_2O component of ~7 wt % was found in the Martian meteorite Zagami by Raman spectroscopy and semi-quantitative chemical analysis, and it was thought to be a solid solution in the $\text{CaAl}_4\text{Si}_2\text{O}_{11}$ – $\text{NaAl}_3\text{Si}_3\text{O}_{11}$ (NAS) system (Beck et al. 2004). This Na end-member, which is called NAS phase in the same manner of calling the Ca end-member, is hypothetically isostructural to CAS phase, and its chemical formula is resulted from a coupled substitution of $\text{Ca}^{2+} + \text{Al}^{3+}$ by $\text{Na}^+ + \text{Si}^{4+}$.

Akaogi et al. (2010) determined the phase relations in the CAS–NAS system by multianvil experiments at pressures of 13–23 GPa and temperatures of 1873 and 2173 K,

Electronic supplementary material The online version of this article (<https://doi.org/10.1007/s00269-020-01106-6>) contains supplementary material, which is available to authorized users.

✉ Youmo Zhou
zhouyoumo201637@gmail.com

- 1 Geodynamics Research Center, Ehime University, Matsuyama 790-8577, Japan
- 2 Earth-Life Science Institute, Tokyo Institute of Technology, Tokyo 152-8550, Japan

and confirmed that CAS–NAS solid solutions can be formed by the above coupled substitution. Furthermore, they reported that the solubility of NAS component in CAS phase has a positive temperature dependence, and the maximum solubility at each temperature likely occurs at the pressure near 23 GPa, which corresponds to the decomposition of $\text{NaAlSi}_2\text{O}_6$ jadeite into NaAlSiO_4 calcium ferrite-type (CF) phase and SiO_2 stishovite. However, the maximum content of NAS component in CAS phase was reported to be 55 mol % at 23 GPa and 2173 K, which is far less than that in the Na-rich CAS phase found in the Zagami meteorite ($\text{Na}/(\text{Na} + \text{Ca}) = 74$ mol %; Beck et al. 2004), and no NAS phase was obtained; instead, the obtained phase assemblages for the NAS composition were jadeite + Al_2O_3 corundum + stishovite and CF phase + corundum + stishovite at 1873 K.

To know whether NAS phase does exist or not, which is an important issue for mineralogy, petrology, and crystallography, we explored the phase relations of the NAS composition by multianvil experiments. According to Akaogi et al. (2010), NAS phase is likely formed at pressures near 23 GPa and temperatures higher than 2273 K, if it does exist. Therefore, we performed experiments in a narrow pressure range around 23 GPa at temperatures of 2373 and 2573 K. Meanwhile, in the same experimental runs, we studied the $\text{NaAlSi}_3\text{O}_8$ (Ab) composition for comparison as well as for evaluating the importance of its phase relations to understand the shock metamorphism of Na-containing feldspars in the shocked meteorites.

It has been found that Na-containing feldspars in some shocked meteorites underwent shock metamorphism and transformed into high-pressure phases (Tomioka and Miyahara 2017). The Na-rich CAS phase mentioned above was derived from labradorite in the shocked Martian meteorites (Beck et al. 2004). El Goresy et al. (2013) proposed decomposition of the Ab composition into NAS phase, stishovite, and a $\text{Na}_2\text{Si}_2\text{O}_5$ melt to speculate the natural occurrence of Na-rich CAS phase, but this reaction has not yet been examined by experiment. On the other hand, oligoclase and albite were found to transform into lingunite (Na-rich hollandite) in some shocked ordinary chondrites (e.g., Gillet et al. 2000), but the mechanism remains under debate (e.g., Kubo et al. 2017), which is partly due to the suspicious existence of lingunite in the phase relations of the Ab composition under equilibrium conditions. We synthesized $\text{K}_{0.2}\text{Na}_{0.8}\text{AlSi}_3\text{O}_8$ hollandite, which is similar to the natural lingunite in terms of Na molar ratio, in the KAlSi_3O_8 – $\text{NaAlSi}_3\text{O}_8$ binary system (Zhou et al. 2017), but this result cannot ensure the stability of lingunite with higher Na contents up to that of the Ab end-member. In the present study, we report new data of the phase relations of the NAS and Ab compositions and discuss some implications for the shock metamorphism of Na-containing feldspars in the shocked meteorites.

Experimental and analytical methods

To make starting materials with the desired bulk compositions, mixtures of SiO_2 , Al_2O_3 , and Na_2CO_3 , were heated in a furnace at 2000 K for 2 h after removing CO_2 at 1273 K for 16 h, and then the products were taken out from the furnace and cooled down fast in air. The obtained Ab starting material was a colorless transparent glass, while the obtained NAS starting material was a milky ceramic pellet. Some tiny fragments of the Ab starting material were analyzed by an energy dispersive X-ray spectrometer (EDS) to confirm the bulk composition. To speculate the bulk composition of the NAS starting material, those of two subsolidus products transformed from the NAS starting material at high pressures and temperatures were measured by EDS using the area mode. The results of these chemical analyses are shown later. Both starting materials were crushed and ground into fine powders and were stored in a furnace at 383 K before use.

Experimental runs were performed in a Kawai-type multianvil apparatus (Orange-2000) installed at Geodynamics Research Center, Ehime University. The high-pressure cell used in the present study is the same as that used by Nomura et al. (2017). Tungsten carbide anvils with 4 mm truncations and Co-doped MgO octahedra were used for pressure generation, and tubular LaCrO_3 heaters were used for temperature generation. Rhenium capsules with the diameter of 1 mm and the height of 0.8 mm were used as sample containers. Pressure calibrations were performed at high temperatures of 1873 and 2273 K (Nomura et al. 2017). Heating temperatures were monitored by a W_{97}Re_3 – $\text{W}_{75}\text{Re}_{25}$ thermocouple, and no correction was applied for the pressure effect on the electromotive force. The uncertainties in pressure and temperature were estimated to be ± 1 GPa and ± 50 –75 K, respectively, following the same criterion mentioned in Nomura et al. (2017). In each run, the high-pressure cell was squeezed slowly until the target load was reached. Then, the temperature was increased to the target value at a rate of ~ 100 K/min and was kept constant under the fixed press load. After certain durations (20–60 min) of constant heating, the runs were quenched to room temperature by shutting down the power supply, and the products were recovered after decompression. Table 1 shows the experimental conditions and results.

The products were embedded in epoxy resin and were polished for subsequent analyses. Phase identification of the subsolidus products was performed with a micro-focus X-ray diffraction (XRD) device (Rigaku MicroMax-007HF) using $\text{Cu-K}\alpha$ radiation. The operation condition was 40 kV and 30 mA. The collimator size was 100 μm . The collected XRD patterns were analyzed using the

Table 1 Experimental conditions and results

Run no.	<i>P</i> (GPa)	<i>T</i> (K)	<i>T</i> (min)	Product
Using the NAS starting material				
OS3671	20.5	(2373)	30	Jd + Cor + St
OS3674	21.5	2373	60	Jd + Cor + St
OS3673	22.5	2373	45	Jd + Cor + St + NAS phase
OS3677	22.5	2373	60	Jd + Cor + St
OS3664	23.5	2373	60	CF + Cor + St
OS3669	22.5	2573	60	NAS phase + Cor + St
OS3662	23.5	2573	20	NAS phase + CF + Cor + St
Using the Ab starting material				
OS3671	20.5	(2373)	30	Jd + St + tr. Cor
OS3674	21.5	2373	60	CF + St
OS3673	22.5	2373	45	CF + St
OS3677	22.5	2373	60	CF + St
OS3664	23.5	2373	60	CF + St
OS3669	22.5	2573	60	Melt + St + NAS phase
OS3662	23.5	2573	20	Melt + St + Cor + CF

Temperature in the bracket was estimated based on the reproducible power-temperature relationships, due to the failure of thermocouple during compression

Jd jadeite, *Cor* corundum, *St* stishovite, *CF* calcium ferrite-type phase, *tr.* trace

software PDIndexer (Seto et al. 2010). Phase identification of the liquidus phases in the partially melted products was made based on the chemical analysis. XRD patterns of the products transformed from the NAS starting material are shown in Fig. 1, and those for the Ab starting material are shown in the electronic supplementary material (Fig. S1). The products were coated with carbon and were observed with a field-emission scanning electron microscope (JEOL JSM7000F) under the working condition of 15 kV and 1 nA. Back-scattered electron images of the products obtained at 2573 K are shown in Figs. 2 and 4, and those for 2373 K are shown in Figs. S2 and S3. Chemical compositions of the starting material and the observed phases (Table 2) were measured with EDS (Oxford Instruments X-Max^N). The point mode was used to analyze the coarse-grained (> 5 μm) phases, except for CF phase, because we found that the focused electron beam seriously damaged the grains of CF phase, which resulted in obvious loss of Na during analysis. Instead, we analyzed the grains of CF phase with electron beam scanning a small area of ~ 1 μm² within individual grains. The area mode was also used to measure the bulk compositions of the starting material, the subsolidus phase assemblages, and the quench crystals in the partially melted products. The quantification standard for Na, Al, and Si is jadeite.

Table 2 shows that the bulk composition of the Ab starting material is almost identical to the ideal chemical

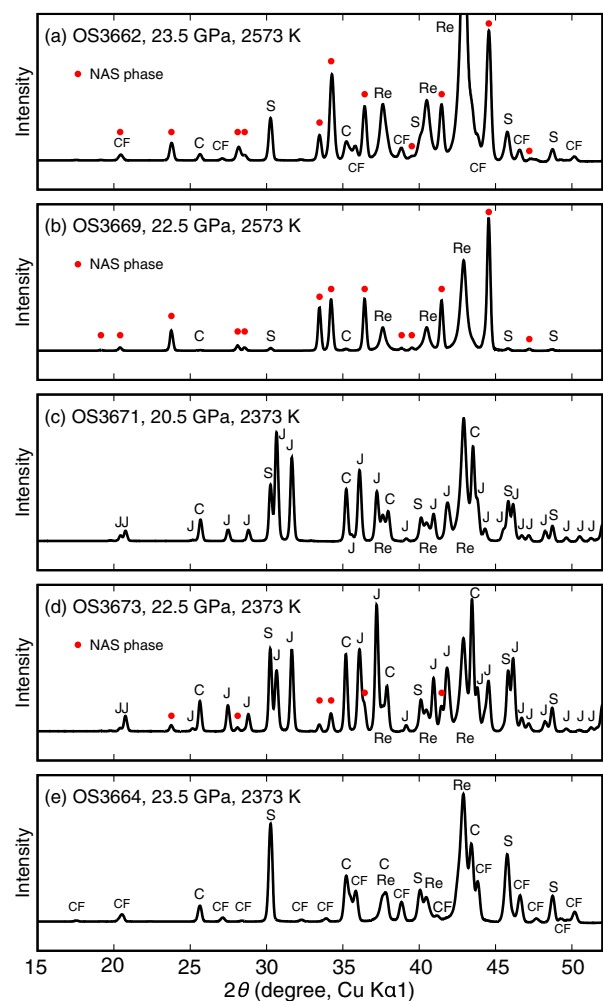
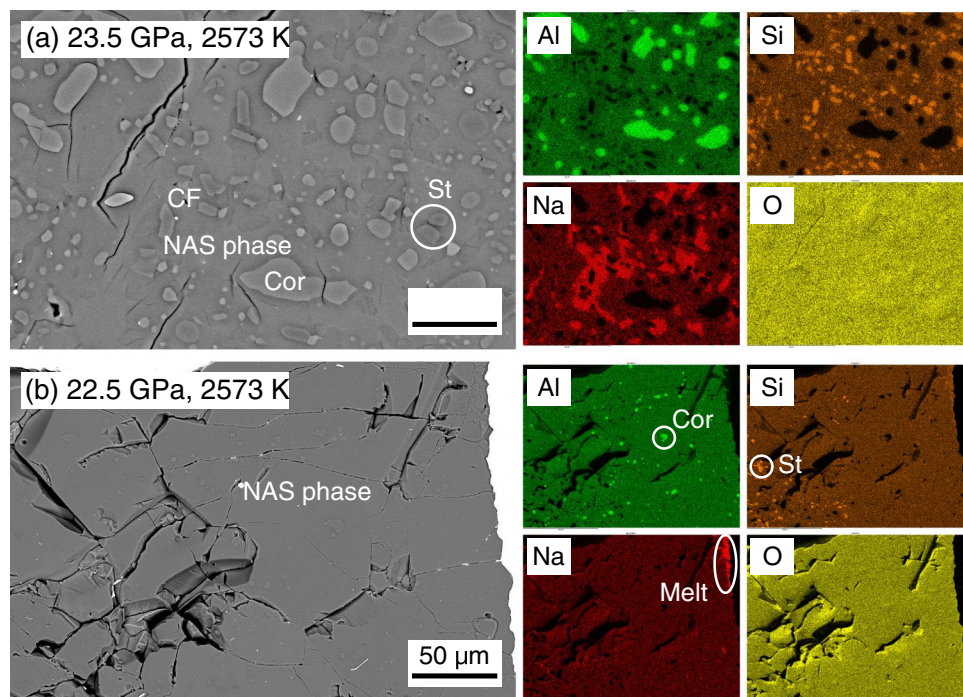


Fig. 1 XRD patterns of the products transformed from the NAS starting material. *J* jadeite, *C* corundum, *S* stishovite, *CF* calcium ferrite-type phase. Due to the small sample sizes relative to the collimator, the capsule material, rhenium, was involved in all the XRD analyses

formula, while that of the NAS starting material, which is inferred to be $\text{Na}_{0.969}\text{Al}_{2.944}\text{Si}_{3.050}\text{O}_{11}$ (OS3664) or $\text{Na}_{0.985}\text{Al}_{2.945}\text{Si}_{3.045}\text{O}_{11}$ (OS3662) from the bulk compositions of the two subsolidus products, contains a few excessive SiO_2 components. This small deviation from the ideal chemical formula was possibly due to the rough surfaces of the multiphase products, which may affect the results of chemical analysis, or it reflects the imperfect chemical homogeneity of the multiphase products. However, even if the deviation is true, it does not affect the conclusions of the present study, because the excessive SiO_2 components just crystallize into additional stishovite at high pressures and temperatures, and stishovite is originally involved in the phase relations.

Fig. 2 Back-scattered electron images and elemental mappings of the products transformed from the NAS starting material at 2573 K. **a** OS3662; **b** OS3669. Abbreviations are the same as those used in Table 1



Results and discussion

Synthesis and identification of NAS phase

The first experimental run OS3662 was performed at 23.5 GPa and 2573 K (Table 1). In the XRD pattern of the product transformed from the NAS starting material (Fig. 1a), we found the diffraction peaks of CF phase, corundum, and stishovite and some unidentified intense peaks. The unidentified peaks were successfully fitted to those based on the crystal structure of CAS phase (Gautron et al. 1999). The back-scattered electron image of the same product shows a multiphase mixture, and the elemental mappings clearly show the grain size and distribution of each phase (Fig. 2a). Table 2 shows that the most dominant phase in this product has a chemical composition of $\text{Na}_{0.989}\text{Al}_{3.001}\text{Si}_{3.002}\text{O}_{11}$, which is just identical to the NAS composition. These results indicate that NAS phase with a hexagonal barium ferrite-type structure has been formed.

Figure 2a shows that NAS phase is in touch with CF phase, corundum, and stishovite, while the latter three phases are not in touch with each other. According to Akaogi et al. (2010), the phase assemblage of CF phase + corundum + stishovite is stable for the NAS composition at 23 GPa and 1873 K. Therefore, the texture shown in Fig. 2a implies the formation of NAS phase at the higher temperature of 2573 K by the reaction between CF phase, corundum, and stishovite. The survival of unreacted phases indicates that the heating duration of 20 min

(Table 1) is probably insufficient for the accomplishment of the slow solid-state reaction.

The heating duration was then extended to 60 min in the second experimental run OS3669 that was performed at 22.5 GPa and 2573 K (Table 1). In the XRD pattern of the product transformed from the NAS starting material, the major peaks are identified to be of NAS phase, with some additional minor peaks of corundum and stishovite (Fig. 1b). This product consists of coarse-grained ($\sim 50\text{--}100\ \mu\text{m}$) NAS phase and small amounts of fine-grained ($< 5\ \mu\text{m}$) corundum and stishovite, as shown in the back-scattered electron image (Fig. 2b). In addition, Na-rich melt in a trace amount can be seen at the hottest corner of the capsule. The Na-rich melt was probably formed by the melting of unreacted Na-rich components at 2573 K and accumulated at the hottest corner of the capsule, which may be avoided, if we can use a completely homogeneous starting material with the NAS composition. In fact, Table 2 shows that the coarse-grained NAS phase, which occupies most parts of the sample, has a chemical composition of $\text{Na}_{0.999}\text{Al}_{3.010}\text{Si}_{2.993}\text{O}_{11}$, which is identical to the NAS composition.

The results of structural analysis suggest that similar to CAS phase, NAS phase probably also has a hexagonal barium ferrite-type structure. The lattice parameters of NAS phase were calculated using the diffraction peaks of NAS phase. Polycrystalline Si was used as the external standard to calibrate the peak positions of NAS phase. To test the reliability of this calibration, the lattice parameters of stishovite were obtained by the same method and were compared with some reference data (Table S1).

Table 2 Chemical compositions of the starting material and the observed phases

Run no.	Phase ^a	Na ₂ O	Al ₂ O ₃	SiO ₂	Total (wt %)	Na	Al	Si	ΣCation ^b
Using the NAS starting material									
OS3671	Jd (21)	14.53 (42)	25.75 (59)	58.72 (86)	98.99 (114)	0.954 (26)	1.028 (21)	1.990 (15)	3.973 (18)
	Cor (19)	–	92.73 (86)	7.71 (24)	100.45 (97)	–	1.828 (5)	0.129 (3)	1.957 (1)
OS3674	Cor (21)	–	98.81 (87)	3.41 (23)	102.22 (89)	–	1.925 (5)	0.056 (4)	1.981 (1)
OS3673	Cor (24)	–	96.48 (76)	5.44 (46)	101.92 (66)	–	1.880 (10)	0.090 (7)	1.970 (2)
OS3677	Cor (27)	–	95.30 (224)	4.77 (111)	100.07 (148)	–	1.893 (26)	0.081 (20)	1.973 (7)
OS3664	Bulk (1)	8.48	42.36	51.73	102.57	0.969	2.944	3.050	6.963
OS3669	NAS phase (29)	8.54 (12)	42.34 (32)	49.62 (44)	100.50 (79)	0.999 (11)	3.010 (11)	2.993 (8)	7.002 (8)
OS3662	Bulk (1)	8.60	42.29	51.54	102.42	0.985	2.945	3.045	6.975
	NAS phase (12)	8.49 (17)	42.37 (44)	49.95 (56)	100.81 (107)	0.989 (15)	3.001 (11)	3.002 (9)	6.992 (11)
	Cor (9)	–	95.29 (108)	6.57 (51)	101.89 (99)	–	1.855 (11)	0.109 (8)	1.963 (3)
Using the Ab starting material									
	Glass* (16)	11.74 (16)	19.04 (16)	67.95 (43)	98.73 (62)	1.006 (11)	0.992 (7)	3.004 (6)	5.003 (9)
OS3671	Jd (21)	14.68 (49)	24.86 (51)	59.05 (106)	98.60 (121)	0.969 (27)	0.997 (23)	2.010 (21)	3.976 (23)
	St (11)	–	0.36 (19)	100.25 (84)	100.61 (74)	–	0.004 (2)	0.997 (2)	1.001 (1)
OS3674	CF (23)	21.15 (84)	36.22 (70)	41.48 (113)	98.85 (147)	0.979 (34)	1.020 (20)	0.990 (21)	2.989 (29)
OS3673	CF (12)	20.86 (46)	35.57 (99)	42.05 (177)	98.48 (106)	0.968 (27)	1.003 (34)	1.006 (32)	2.977 (29)
	St (14)	–	0.50 (13)	100.78 (99)	101.32 (91)	–	0.006 (2)	0.995 (2)	1.002 (2)
OS3677	CF (32)	20.98 (79)	35.12 (73)	41.52 (128)	97.62 (153)	0.983 (34)	1.001 (21)	1.004 (23)	2.004 (6)
	St (22)	–	0.36 (13)	99.01 (73)	99.38 (74)	–	0.004 (2)	0.997 (1)	1.001 (0)
OS3664	CF (28)	20.99 (57)	35.37 (53)	41.31 (104)	97.66 (96)	0.984 (25)	1.008 (19)	0.998 (18)	2.990 (21)
	St (24)	–	0.36 (15)	97.99 (68)	98.38 (74)	–	0.004 (2)	0.997 (2)	1.001 (0)
OS3669	Melt (10)	20.15 (62)	21.39 (37)	57.57 (82)	99.12 (57)	1.133 (40)	0.731 (12)	1.669 (15)	3.532 (31)
	St (16)	–	0.41 (8)	100.75 (60)	101.18 (59)	–	0.005 (1)	0.996 (1)	1.001 (1)
	NAS phase (15)	8.66 (34)	42.54 (75)	50.03 (97)	101.24 (200)	1.005 (25)	3.003 (13)	2.997 (9)	7.005 (18)
OS3662	Melt (1)	18.13	23.43	56.84	98.40	1.018	0.800	1.646	3.463
	St (17)	–	0.54 (8)	100.58 (67)	101.12 (65)	–	0.006 (1)	0.995 (1)	1.002 (0)
	Cor (10)	–	92.46 (48)	8.61 (16)	101.07 (52)	–	1.809 (3)	0.143 (2)	1.952 (1)
	CF (18)	21.15 (55)	35.94 (73)	41.94 (83)	99.03 (205)	0.977 (8)	1.009 (6)	0.999 (5)	2.985 (6)

Abbreviations are the same to those used in Table 1

^aNumbers in the brackets represent the amounts of analyses

^bThe oxygen numbers are fixed to 6 for Jd, 4 for CF, 11 for NAS phase, 3 for Cor, 2 for St, 5 for Melt, and 8 for the glass

* Glass with the NaAlSi₃O₈ composition is the second starting material in the present study. See more details in the main text

It can be seen that stishovite, except for that coexisting with CF phase, has lattice parameters comparable to the data reported previously. The lattice parameters of NAS phase were calculated to be $a = 5.3565$ (2) Å, $c = 12.6732$ (17) Å, $V = 314.90$ (5) Å³ (OS3662) and $a = 5.3534$ (3) Å, $c = 12.6942$ (7) Å, $V = 315.06$ (4) Å³ (OS3669), using 10 and 17 diffraction peaks of NAS phase in the XRD patterns shown in Fig. 1a, b, respectively. The observed and calculated values of d spacing of NAS phase are shown in Table 3. A comparison is made between CAS phase, NAS phase, and their solid solutions in the lattice parameters (Table S2 and Fig. 3). Our two results of NAS phase are comparable to each other, and the lattice parameters are significantly smaller than those of CAS phase and the solid solutions. In contrast, Akaogi et al. (2009) reported the

shortest c -axis length of CAS phase among those reported previously, which is close to the c -axis lengths of NAS phase. Furthermore, Akaogi et al. (2010) observed an increase of c -axis length of the CAS–NAS solid solution with increasing NAS component, which is contradicted by the shorter c axis of NAS phase. With respect to the ionic radii, Na⁺ (1.39 Å for 12-fold coordination) is comparable to Ca²⁺ (1.34 Å), while Si⁴⁺ (0.400 Å for octahedral coordination) is obviously smaller than Al³⁺ (0.535 Å) (Shannon 1976). Therefore, if only the effect of ionic radius works on the lattice parameters, the coupled substitution of Ca²⁺ + Al³⁺ by Na⁺ + Si⁴⁺ should cause the shorter a and c axes and smaller unit cell of the crystal structure of NAS phase, as observed in the present study.

Table 3 XRD data of NAS phase

<i>H</i>	<i>k</i>	<i>l</i>	<i>d</i> _{observed} (Å)	<i>d</i> _{calculated} (Å)	Intensity
0	1	0	4.6326	4.6362	< 1
0	1	1	4.3513	4.3548	2
0	1	2	3.7429	3.7438	15
0	0	4	3.1738	3.1735	4
0	1	3	3.1244	3.1254	2
1	1	0	2.6766	2.6767	32
0	1	4	2.6187	2.6188	38
1	1	2	2.4655	2.4663	39
0	2	0	2.3173	2.3181	2
0	2	1	2.2799	2.2804	2
0	1	5		2.2268	
0	2	2	2.1769	2.1774	38
0	0	6		2.1157	
1	1	4		2.0461	
0	2	3	2.0329	2.0330	100
0	1	6	1.9245	1.9247	< 1
0	2	4		1.8719	
1	2	0		1.7523	
1	2	1		1.7358	
0	2	5	1.7117	1.7119	2
1	2	2		1.6891	
0	1	7	1.6890	1.6888	2
1	1	6	1.6600	1.6598	< 1
1	2	3		1.6190	
0	0	8	1.5865	1.5868	3
0	2	6	1.5627	1.5627	71
0	3	0	1.5454	1.5454	7
0	3	1	1.5339	1.5340	49
1	2	4		1.5340	
0	3	2	1.5014	1.5015	16
0	1	8		1.5013	
0	3	3		1.4516	
1	2	5	1.4421	1.4421	< 1
0	2	7		1.4283	
0	3	4		1.3894	
1	1	8		1.3650	
1	2	6		1.3495	
0	1	9		1.3494	
2	2	0	1.3384	1.3383	77
0	3	5		1.3201	
2	2	2		1.3095	
0	2	8	1.3095	1.3094	20
1	3	0		1.2858	
1	3	1		1.2793	
0	0	10		1.2694	
1	3	2		1.2602	
1	2	7		1.2601	
0	3	6		1.2479	
2	2	4		1.2332	
1	3	3		1.2303	
0	1	10	1.2243	1.2243	8
0	2	9	1.2051	1.2049	12

Table 3 (continued)

Run OS3669: hexagonal, $a=5.3534$ (3) Å, $c=12.6942$ (7) Å, $V=315.06$ (4) Å³

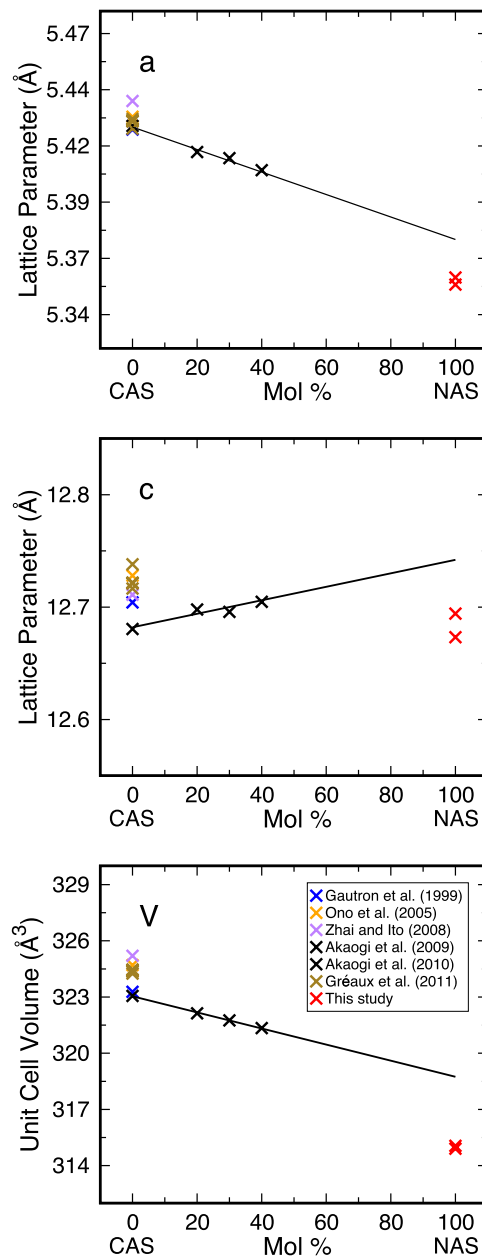


Fig. 3 Lattice parameters of CAS phase, NAS phase, and their solid solutions. The vertical error bars are shorter than the sizes of the cross symbols, except those of the data points of Ono et al. (2005)

Phase relations of $\text{NaAl}_3\text{Si}_3\text{O}_{11}$ and $\text{NaAlSi}_3\text{O}_8$

The experimental results obtained using the NAS starting material are shown in Table 1. At 2373 K, the phase assemblage of jadeite + corundum + stishovite was formed at 20.5, 21.5, and 22.5 GPa (Fig. 1c, d, and Fig. S2a–d), and that of CF phase + corundum + stishovite was formed at 23.5 GPa (Fig. 1e and Fig. S2e). These phase assemblages are consistent with the results of Akaogi et al. (2010) obtained at a much lower temperature of 1873 K. We noted that some diffraction peaks of NAS phase appear in addition to those of jadeite, corundum, and stishovite in the XRD pattern of the phase assemblage recovered in the experimental run OS3673 at 22.5 GPa and 2373 K (Fig. 1d). However, only few grains were identified as NAS phase under the electron microscopic observation, because they were hardly highlighted by the elemental mappings, which is possibly due to the relatively small chemical contrast between jadeite and NAS phase, as well as the low volume fraction of NAS phase in the product. The run OS3677 was performed at 22.5 GPa and 2373 K as a repeat of the run OS3673 (Table 1) for confirmation of the four-phase coexistence, but NAS phase was not confirmed in the phase assemblage of jadeite + corundum + stishovite. The results of these two runs indicate that this pressure and temperature condition is so close to or just located on the phase boundary. At 2573 K, NAS phase was formed at 22.5 and 23.5 GPa, as described above in detail. The experimental results obtained using the NAS starting material reveal the phase relations rather clearly, although the phase boundaries were not well constrained, as shown in Fig. 5a.

Although no single-phase product of NAS phase was obtained, due to the slow solid-state reactions, the dominant formation of NAS phase in the two products (Table 1: OS3662 and OS3669; Fig. 2) indicates that NAS phase was formed in its thermodynamic stability region. The stability region of NAS phase is much narrower than that of CAS phase (Ishibashi et al. 2008; Zhai and Ito 2008; Akaogi et al. 2009), because NAS phase is stable only at temperatures above 2373 K around 23 GPa, and the incorporation of NAS component in CAS phase narrows down the stability region of CAS phase (Akaogi et al. 2010). Owing to the very high stability temperature, NAS phase can hardly exist in the mantle under the typical geotherm.

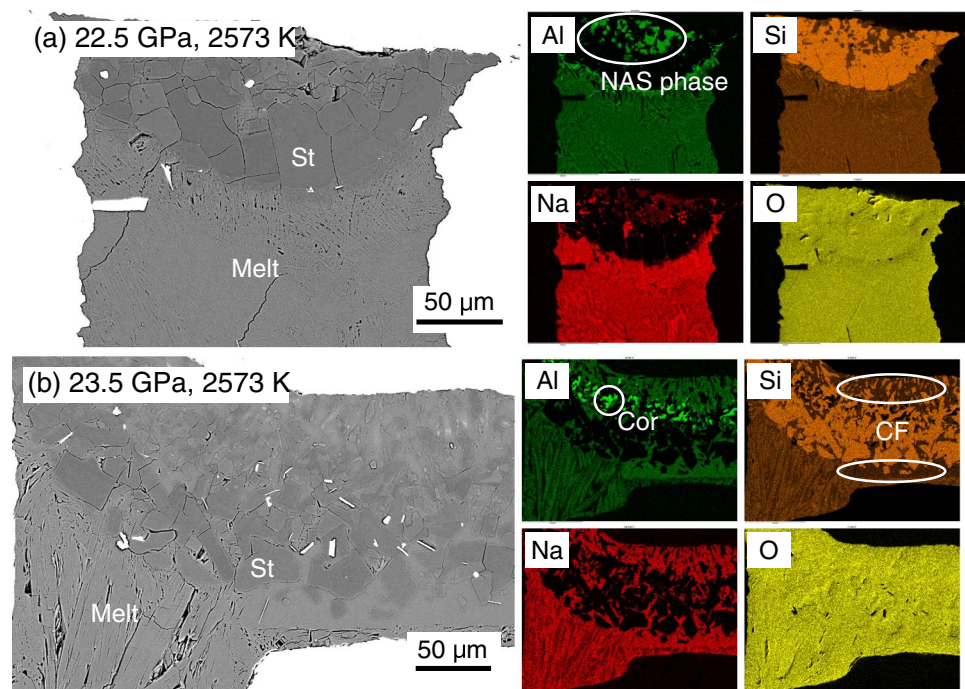
In all the products transformed from the NAS starting material, stishovite has grain sizes of ~1–3 μm (Fig. 2 and Fig. S2). Such small grain sizes prohibit a reliable chemical analysis on the stishovite grains. Meanwhile, in most of the phase assemblages of jadeite + corundum + stishovite and CF phase + corundum + stishovite, the grains of the two Na-containing phases always contain many dispersive fine-grained (< 1 μm) inclusions of corundum and stishovite (Fig. S2). These textures also invalidate any reliable chemical analysis. Only jadeite grains in the phase

assemblage obtained in the run OS3671 (Fig. S2a) were analyzed by EDS, of which the chemical compositions were found to slightly deviate from the ideal composition (Table 2). Corundum grains in most of the products transformed from the NAS starting material are large enough (~5 μm) for a reliable chemical analysis (Fig. 2a and Fig. S2a–d), which were found to contain ~3–8 wt% SiO_2 components (Table 2).

The experimental results obtained using the Ab starting material are shown in Table 1. At 2373 K, the phase assemblage of jadeite + stishovite was formed at 20.5 GPa (Figs. S1a and S3a), while that of CF phase + stishovite was formed at 21.5, 22.5, and 23.5 GPa (Figs. S1b and S3b–e). At 22.5 GPa and 2573 K, a partial melting occurred, as clearly shown by the layered texture as well as the needle-shaped quench crystals (Fig. 4a). The first liquidus phase is stishovite, and the second liquidus phase is NAS phase, as indicated by the textural observation and the obtained chemical compositions (Table 2). At 23.5 GPa and 2573 K, another partial melting occurred, where the first liquidus phase is stishovite, and the second liquidus phase is corundum (Table 2 and Fig. 4b). In this sample, we found CF phase in addition, which is not only located at the coldest place of the capsule but also in touch with the quench crystals. The phase assemblage of CF phase + stishovite is stable for the Ab composition under the subsolidus condition. Therefore, the four-phase coexistence of melt, stishovite, corundum, and CF phase probably violates the Gibbs phase rule. In the phase assemblage of CF phase + stishovite, CF phase should be the solidus phase, and the reasonable phase assemblage which can occur above the solidus temperature should be melt + stishovite + corundum. The survival of CF phase is probably due to the existence of thermal gradient in the capsule. On the other hand, the occurrence of NAS phase at 22.5 GPa and corundum at 23.5 GPa in the partially melted phase assemblages indicates that CF phase undergoes incongruent melting above the solidus temperature. Based on the experimental results obtained using the Ab starting material, the phase boundaries were tentatively estimated, as shown in Fig. 5b.

In all the products transformed from the Ab starting material, the grains of jadeite and CF phase have chemical compositions close to the ideal chemical formulas, and stishovite contains Al_2O_3 components less than 0.5 wt % (Table 2). The bulk chemical compositions of the two melts are $\text{Na}_{1.133}\text{Al}_{0.731}\text{Si}_{1.667}\text{O}_5$ and $\text{Na}_{1.018}\text{Al}_{0.800}\text{Si}_{1.646}\text{O}_5$ for the runs OS3669 at 22.5 GPa and OS3662 at 23.5 GPa, respectively (Table 2). El Goresy et al. (2013) proposed decomposition of the Ab composition into NAS phase, stishovite, and a $\text{Na}_2\text{Si}_2\text{O}_5$ melt. This phase assemblage is confirmed by our experimental result obtained at 22.5 GPa and 2573 K, but the chemical composition of the obtained melt is quite different from that assumed by El Goresy et al. (2013).

Fig. 4 Back-scattered electron images and elemental mappings of the products transformed from the Ab starting material at 2573 K. **a** OS3669; **b** OS3662. Abbreviations are the same as those used in Table 1



Implications for the shock metamorphism of Na-containing feldspars in the shocked meteorites

Phase relations determined by static high-pressure experiments are frequently used as the references to estimate the formation conditions of the high-pressure phases discovered in the shocked meteorites. Akaogi et al. (2010) suggested that the natural Na-rich CAS phase (Beck et al. 2004) crystallized in a pressure range around 22 GPa at temperatures close to or higher than ~2273–2473 K, by linearly extrapolating the solubility of NAS component in CAS phase to higher values at higher temperatures. In contrast, we have synthesized NAS phase around 23 GPa at temperatures of 2373 and 2573 K, which suggests that the CAS–NAS solid solution with a Na/Ca ratio similar to that of the natural Na-rich CAS phase (74:26) can probably be stabilized around 23 GPa at temperatures lower than 2373–2573 K. Therefore, the temperature of 2473 K was slightly overestimated by Akaogi et al. (2010) to speculate the lower bound of formation temperature of the natural Na-rich CAS phase.

On the other hand, Beck et al. (2004) showed the texture of the natural Na-rich CAS phase that euhedral grains of CAS phase are intergrown with needle-shaped grains of stishovite in the melt pockets made from labradorite, and the grain size shows a cooling texture with grain size decreasing from core to rim of the phase assemblage. They therefore suggested that the phase assemblage of Na-rich CAS phase + stishovite is diagnostic of melting. El Goresy et al. (2013) further suggested the quenching of Na-rich CAS

phase + stishovite from a high-pressure labradorite melt at ~22 GPa and ~2173–2473 K. By using the Ab composition, we obtained the phase assemblage of melt + stishovite + NAS phase at 22.5 GPa and 2573 K, which is very similar to that observed in the melt pockets of the Martian meteorites. However, it should be noted that our result is a partial melting under the equilibrium condition, while the natural case is a rapid crystallization of a high-pressure labradorite melt during quenching. Our result shows that stishovite and NAS phase are the residual solid phases in the partial melting of the Ab composition. This result is supportive to the previous inference that Na-rich CAS phase and stishovite crystallized together from a high-pressure labradorite melt during quenching. If labradorite was completely melted at ~22 GPa in the shock events, the peak temperature should be higher than 2373 K, according to the solidus temperature of the Ab composition (Fig. 5b). However, for further quantitative understanding of the melting behavior of labradorite in the shock events, it is necessary to focus on the natural labradorite compositions rather than the end-members, because the high content of anorthite (~50 mol %) in labradorite may have some significant influence.

Shock metamorphism of oligoclase and albite in the shocked ordinary chondrites is also an interesting issue, but has not yet been well understood (Tomioka and Miyahara, 2017). One of the unsolved issues is the stability of $\text{NaAlSi}_3\text{O}_8$ lingunite, which was firstly reported by the diamond anvil cell experiment on the Ab composition (Liu 1978), but has not yet been confirmed at temperatures up to 2273 K in the subsequent studies (e.g., Akaogi et al. 2010).

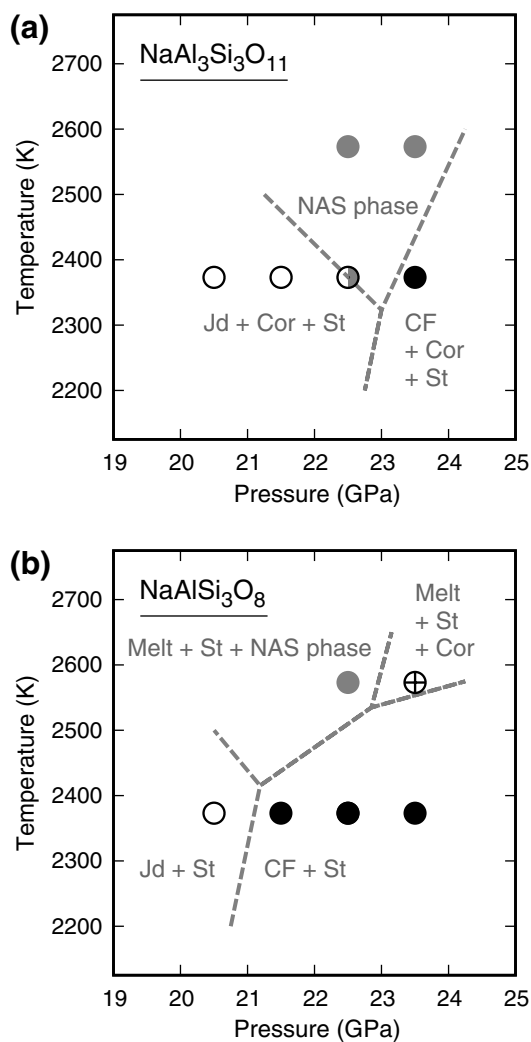


Fig. 5 Phase diagrams of $\text{NaAl}_3\text{Si}_3\text{O}_{11}$ and $\text{NaAlSi}_3\text{O}_8$. Abbreviations are the same as those used in Table 1. **a** The hollow circles represent the phase assemblage of Jd + Cor + St; the half-filled circle represents Jd + Cor + St + NAS phase; the solid black circle represents CF + Cor + St; the solid grey circles represent NAS phase + unreacted phases. The details about these data points have been clearly described in the main text. **b** The hollow circle represents Jd + St; the solid black circles represent CF + St; the solid grey circle represents melt + St + NAS phase; the circle with cross represents melt + St + Cor, and note that CF phase was also found in this product, as clearly mentioned in the main text

In the present study, we explored the phase relations of the Ab composition around 23 GPa at higher temperatures of 2373 and 2573 K, which further suggest that $\text{NaAlSi}_3\text{O}_8$ lingunite is unlikely a thermodynamically stable phase (Fig. 5b). Therefore, a metastable formation by solid-state transformation or liquid crystallization may explain the natural occurrence of lingunite. In addition, although the contents are not high, the orthoclase and anorthite components in oligoclase and albite may have key effects on the formation of lingunite in the shock events (Kubo et al. 2017).

Melting of oligoclase and albite has also been usually observed in the melt pockets or near the shock veins of the shocked ordinary chondrites (e.g., Chen and El Goresy, 2000). The pressure condition generated in the shock veins was estimated to be around 23 GPa, based on the formation of majorite-pyropo garnet and magnesiowüstite in the shock veins by the partial melting of the bulk rock (e.g., Chen et al. 1996). If the melting of oligoclase and albite also occurred around 23 GPa, the peak temperature generated in these feldspars should be higher than 2373 K for complete melting, as suggested by our results (Fig. 5b). However, for further precise estimation, the effects of orthoclase and anorthite components on the melting behavior of oligoclase and albite should be studied. In addition, our results show that stishovite, NAS phase, and corundum can be formed in the partial melting of the Ab composition around 23 GPa. Although these phases have not been discovered in oligoclase or albite grains of the shocked ordinary chondrites, they may be found in the shocked ordinary chondrites associated with the partial melting of Na-rich feldspars, because the pressure and temperature conditions generated in the shocked mineral grains can be quite variable.

Funding This work was supported by the Grand-in-Aid for Scientific Research on Innovative Areas (No. 15H5829) to Tetsuo Irifune.

Compliance with ethical standards

Conflict of Interest The authors declare that they have no conflict of interest.

References

- Akaogi M, Haraguchi M, Yaguchi M, Kojitani H (2009) High-pressure phase relations and thermodynamic properties of $\text{CaAl}_4\text{Si}_2\text{O}_{11}$ CAS phase. *Phys Earth Planet Inter* 173:1–6. <https://doi.org/10.1016/j.pepi.2008.10.010>
- Akaogi M, Haraguchi M, Nakanishi K, Ajiro H, Kojitani H (2010) High-pressure phase relations in the system $\text{CaAl}_4\text{Si}_2\text{O}_{11}$ - $\text{NaAl}_3\text{Si}_3\text{O}_{11}$ with implication for Na-rich CAS phase in shocked Martian meteorites. *Earth Planet Sci Lett* 289:503–508. <https://doi.org/10.1016/j.epsl.2009.11.043>
- Beck P, Gillet P, Gautron L, Daniel I, El Goresy A (2004) A new natural high-pressure (Na, Ca)-hexaluminosilicate [$(\text{Ca}_x\text{Na}_{1-x})\text{Al}_3 + x\text{Si}_3 - x\text{O}_{11}$] in shocked Martian meteorites. *Earth Planet Sci Lett* 219:1–12. [https://doi.org/10.1016/S0012-821X\(03\)00695-2](https://doi.org/10.1016/S0012-821X(03)00695-2)
- Chen M, El Goresy A (2000) The nature of maskelynite in shocked meteorites: not diaplectic glass but a glass quenched from shock-induced dense melt at high pressures. *Earth Planet Sci Lett* 179:489–502. [https://doi.org/10.1016/S0012-821X\(00\)00130-8](https://doi.org/10.1016/S0012-821X(00)00130-8)
- Chen M, Sharp TG, El Goresy A, Wopenka B, Xie X (1996) The majorite-pyropo + magnesiowüstite assemblage: constraints on the history of shock veins in chondrites. *Science* 271:1570–1573. <https://doi.org/10.1126/science.271.5255.1570>
- El Goresy A, Gillet P, Miyahara M, Ohtani E, Ozawa S, Beck P, Montagnac G (2013) Shock-induced deformation of Shergottites:

- shock-pressures and perturbations of magmatic ages on Mars. *Geochim Cosmochim Acta* 101:233–262. <https://doi.org/10.1016/j.gca.2012.10.002>
- Gautron L, Angel RJ, Miletich R (1999) Structural characterization of the high-pressure phase $\text{CaAl}_4\text{Si}_2\text{O}_{11}$. *Phys Chem Miner* 27:47–51. <https://doi.org/10.1007/s002690050239>
- Gillet P, Chen M, Dubrovinsky L, El Goresy A (2000) Natural $\text{NaAlSi}_3\text{O}_8$ -hollandite in the shocked Sixiangkou meteorite. *Science* 287:1633–1636. <https://doi.org/10.1126/science.287.5458.1633>
- Gréaux S, Nishiyama N, Kono Y, Irifune T, Gautron L (2011) P-V-T equation of state of $\text{CaAl}_4\text{Si}_2\text{O}_{11}$ CAS phase. *Phys Chem Miner* 38:581–590. <https://doi.org/10.1007/s00269-011-0430-7>
- Hirose K, Fei Y (2002) Subsolvus and melting phase relations of basaltic composition in the uppermost lower mantle. *Geochim Cosmochim Acta* 66:2099–2108. [https://doi.org/10.1016/S0016-7037\(02\)00847-5](https://doi.org/10.1016/S0016-7037(02)00847-5)
- Irifune T, Ringwood AE, Hibberson WO (1994) Subduction of continental crust and terrigenous and pelagic sediments: an experimental study. *Earth Planet Sci Lett* 126:351–368. [https://doi.org/10.1016/0012-821X\(94\)90117-1](https://doi.org/10.1016/0012-821X(94)90117-1)
- Ishibashi K, Hirose K, Sata N, Ohishi Y (2008) Dissociation of CAS phase in the uppermost lower mantle. *Phys Chem Miner* 35:197–200. <https://doi.org/10.1007/s00269-007-0212-4>
- Ishii T, Kojitani H, Akaogi M (2012) High-pressure phase transitions and subduction behavior of continental crust at pressure-temperature conditions up to the upper part of the lower mantle. *Earth Planet Sci Lett* 357–358:34–41. <https://doi.org/10.1016/j.epsl.2012.09.019>
- Kubo T, Kono M, Imamura M, Kato T, Uehara S, Kondo T, Higo Y, Tange Y, Kikegawa T (2017) Formation of a metastable hollandite phase from amorphous plagioclase: a possible origin of lingunite in shocked chondritic meteorites. *Phys Earth Planet Inter* 272:50–57. <https://doi.org/10.1016/j.pepi.2017.09.006>
- Kuwahara H, Nomura R, Nakada R, Irifune T (2018) Simultaneous determination of melting phase relations of mantle peridotite and mid-ocean ridge basalt at the uppermost lower mantle conditions. *Phys Earth Planet Inter* 284:36–50. <https://doi.org/10.1016/j.pepi.2018.08.012>
- Liu L (1978) High-pressure phase transformations of albite, jadeite and nepheline. *Earth Planet Sci Lett* 37:438–444. [https://doi.org/10.1016/0012-821X\(78\)90059-6](https://doi.org/10.1016/0012-821X(78)90059-6)
- Nishi M, Gréaux S, Tateno S, Kuwayama Y, Kawai K, Irifune T, Maruyama S (2018) High-pressure phase transitions of anorthositic crust in the Earth's deep mantle. *Geosci Front* 9:1859–1870. <https://doi.org/10.1016/j.gsf.2017.10.002>
- Nomura R, Zhou Y, Irifune T (2017) Melting phase relations in the MgSiO_3 - CaSiO_3 system at 24 GPa. *Prog Earth Planet Sci* 4:34. <https://doi.org/10.1186/s40645-017-0149-2>
- Ono S, Iizuka T, Kikegawa T (2005) Compressibility of the calcium aluminosilicate, CAS, phase to 44 GPa. *Phys Earth Planet Inter* 150:331–338. <https://doi.org/10.1016/j.pepi.2004.12.001>
- Seto Y, Nishio-Hamane D, Nagai T, Sata N (2010) Development of a software suite on X-ray diffraction experiments. *Rev High Press Sci Technol* 20:269–276. <https://doi.org/10.4131/jshpreview.20.269>
- Shannon RD (1976) Revised effective ionic radii and systematic studies of interatomic distances in halides and chalcogenides. *Acta Cryst A* 32:751–767. <https://doi.org/10.1107/S0567739476001551>
- Tomioka N, Miyahara M (2017) High-pressure minerals in shocked meteorites. *Meteorit Planet Sci*. <https://doi.org/10.1111/maps.12902>
- Wang W, Takahashi E (1999) Subsolvus and melting experiments of a K-rich basaltic composition to 27 GPa: implication for the behavior of potassium in the mantle. *Am Miner* 84:357–361. <https://doi.org/10.2138/am-1999-0319>
- Zhai S, Ito E (2008) Phase relations of $\text{CaAl}_4\text{Si}_2\text{O}_{11}$ at high-pressure and high-temperature with implications for subducted continental crust into the deep mantle. *Phys Earth Planet Inter* 167:161–167. <https://doi.org/10.1016/j.pepi.2008.03.004>
- Zhou Y, Irifune T, Ohfuji H, Shinmei T, Du W (2017) Stability region of $\text{K}_{0.2}\text{Na}_{0.8}\text{AlSi}_3\text{O}_8$ hollandite at 22 GPa and 2273 K. *Phys Chem Miner* 44:33–42. <https://doi.org/10.1007/s00269-016-0834-5>

Publisher's Note Springer Nature remains neutral with regard to jurisdictional claims in published maps and institutional affiliations.